EasyChair Preprint

№ 426

Closed-form freehand 3D ultrasound spatial calibration based on N-wedge phantom

Yanping Lin, Zhenhuan Wang, Xiaojie Guo, Huixiang Wang and Fang Wang

August 14, 2018

Closed-form freehand 3D ultrasound spatial calibration based on N-wedge phantom

Yanping Lin[1], Zhenhuan Wang[1], Xiaojie Guo[1], Huixiang Wang[2], Fang Wang [2]*

[1]Institute of Biomedical Manufacturing and Life Quality Engineering, State Key Laboratory of Mechanical System and Vibration, School of Mechanical Engineering, Shanghai Jiao Tong University, Shanghai 200240, China

[2]Department of Orthopedics, Shanghai Jiao Tong University First People's Hospital, Shanghai 200080, China

Keywords: freehand 3D ultrasound, ultrasound calibration, N-wedge phantom, closed-form

Abstract

Freehand 3D ultrasound imaging system has many applications in healthcare. The purpose of ultrasound calibration is to determine the transformation matrix from the ultrasound probe coordinate system to the ultrasound image coordinate system. In this study, we propose a variant of the widely used N-wire phantom called the N-wedge phantom, which is a combination phantom of wires and wedges. Prototypes of the two phantoms were produced, and we compared the N-wedge phantom and N-wire phantom in terms of their precision, accuracy, calibration time, ease of use, and ease of manufacture. The mean values of the precision of the N-wedge phantom and N-wire phantom at the center point are 0.67 mm and 0.74 mm, respectively, while the mean values of the accuracy of the phantoms are 1.73 mm and 1.89 mm, respectively. Calibration using the two phantoms can meet the requirements for medical application; however, the N-wedge phantom is easier to use and can be manufactured without sacrificing precision and accuracy.

1 Introduction

Ultrasound imaging is widely used in medical diagnosis and adjuvant therapy because it is inexpensive, nonionizing, easy to use, and the images are captured real-time. Recently, three-dimensional (3D) ultrasound imaging is increasingly used in many applications owing to the following limitations of the traditional two-dimensional (2D) ultrasound imaging. First, 2D ultrasound images can only provide some cross-sectional images of the human body, and clinicians have to reconstruct the 3D structure of human organs based on their experiences, which is a time-consuming, inefficient, and subjective process. Second, 2D ultrasound images can only estimate human organs and tumors with a rectangular or ellipsoid; however, 3D ultrasound images can make up for these deficiencies by providing detailed information about human organs and tumors. There are currently four different techniques to acquire 3D ultrasound image: mechanical scanners, freehand scanning with position sensing, freehand scanning without position sensing, and 2D arrays for dynamic 3D ultrasound. Among these techniques, freehand 3D ultrasound image with position sensing is widely used owing to its unrestricted data acquisition range [1]. In freehand 3D ultrasound technology, the system collects data while the probe moves freely. When the ultrasound probe moves to scan human organs, the position sensor fixed on the probe records position information of the probe. After collecting a series of 2D ultrasound images, 3D ultrasound image can be acquired using 3D reconstruction algorithm. Finally, the system uses a visualization technique to display 3D ultrasound image [2]. Freehand 3D ultrasound technology can provide more detailed information compared to a 2D ultrasound image. It also has the advantage of small size and observes the lesion area at any angle. Thus, it is widely used in surgical navigation, computer assisted surgery, complex organ visualization and analysis [3].

The spatial location and direction information of 2D ultrasound image need to be acquired in 3D ultrasound applications. Typically, the optical position sensor fixed on the ultrasound probe can track the spatial position of the ultrasound probe. However, it is not sufficient to determine the location of every 2D ultrasound image using only the location of the ultrasound probe. The ultrasound probe should be calibrated accurately so that the spatial relationship between the ultrasound image coordinate system and the ultrasound probe coordinate system is determined in the process and the transformation matrix is also acquired. Therefore, ultrasound probe calibration is very important in freehand 3D ultrasound image applications.

In recent years, freehand 3D ultrasound calibration has been an active research topic [2, 4]. Typically, the ultrasound probe is used to scan a phantom to complete the process. According to different calibration principles, the existing phantoms are mainly divided into four categories: point phantom, wire phantom, plane phantom, and calibration without phantom. The point phantom usually uses the intersection point of a pair of crossed lines [5] or the center of a sphere as the target [6, 7]. Some point phantoms have more than one target in a single ultrasound image [8]. The wire phantoms include three-wire phantom, which is composed of three perpendicular lines [9, 10], and N-wire phantom, which has several pairs of parallel lines [11–14]. Some researchers have also used plane phantoms [15–19]. Furthermore, calibration methods without phantom have been proposed by some researchers [20, 21].

Among the above-mentioned phantoms, the N-wire phantom is widely used. The N-wire geometry was initially used for image registration and subsequently used in other domains, such as ultrasound calibration and robotics, to compute transformation [22]. Calibration methods based on the N-wire phantom have widely studied [11–13, 23], and most of these

phantoms were manufactured using wires. It has been reported that it is difficult to accurately locate the actual intersection points of the ultrasound image planes and the wires [13]. The wire appearance is determined by the ultrasound axial and lateral resolutions. The appearance of nylon wires of different diameters yields different images at the ultrasound scan-plane focal depth. Thus, it is difficult to accurately locate these points. However, the N-wire phantom is still a compelling choice for ultrasound calibration owing to its unique geometric structure and it can realize automatic image segmentation algorithm.

In this paper, freehand ultrasound calibration based on a new phantom called the N-wedge phantom is presented. The N-wedge phantom not only has the same principle as the N-wire phantom, but also has the advantage of the plane-phantom. Experiments were conducted to compare the calibration factors of the proposed N-wedge phantom with those of the traditional N-wire phantom in terms of their precision, accuracy, image segmentation time, ease of use, and ease of manufacture. Reasons for errors in different calibration methods and various factors to be considered in the calibration process were discussed.

2. Materials and Methods

2.1 System overview

This section presents high-level overview of our ultrasound calibration system. The system includes both the hardware and software.

2.1.1 Hardware configuration

The hardware configuration of the calibration system includes the Polaris Vicra optical tracker system (Northern Digital Inc., Waterloo, Canada), Sonostar ultrasound system (Sonostar, Guangzhou, China), 7.5 MHz linear series wireless transducer (Sonostar, Guangzhou, China), N-wedge phantom, N-wire phantom, stylus, some passive markers, and sink, as shown in Fig. 1.

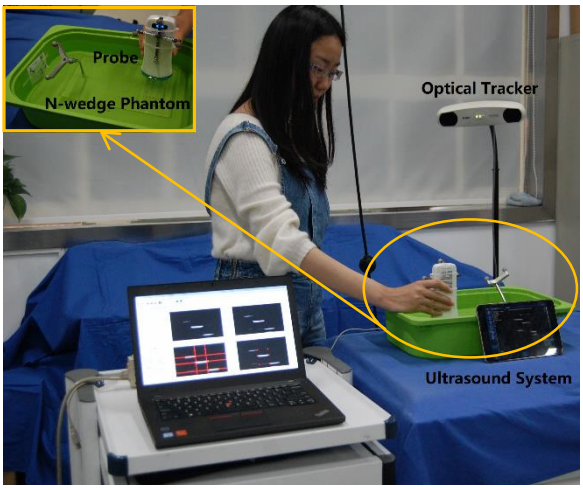

Fig. 1 Hardware configurations of the ultrasound calibration system

2.1.2 Software design

The software of the calibration system was developed using widely used open source toolkits in medical applications such as Visualization Toolkit (VTK), Insight Toolkit (ITK), Image Guided Surgery Toolkit (IGSTK), Open Source Computer Vision (OpenCV), Qt, and Microsoft DirectShow.

2.2 Mathematic framework

The principle of the N-wedge is illustrated as follows.

Definitions:

p^A denotes the coordinates of p in a coordinate system A;

$\mathbf{T}_{A\leftarrow B}$ represents a homogeneous transformation that maps p^B to p^A, as in $p^A = \mathbf{T}_{A\leftarrow B}\, p^B$;

W is the world coordinate system defined in the optical tracker system;

S is the sensor coordinate system defined in the position sensor attached to the ultrasound probe;

P is the phantom coordinate system defined in the reference markers attached to the phantom;

I is the ultrasound image coordinate system.

The purpose of ultrasound calibration is to find $\mathbf{T}_{S\leftarrow I}$, which is the transformation from the ultrasound image coordinate system to the ultrasound probe coordinate system. The transformations $\mathbf{T}_{W\leftarrow S}$ and $\mathbf{T}_{W\leftarrow P}$ can be directly read from the optical tracking system. For the point p in the phantom, if its coordinates are both known in the image frame and phantom frame, we obtain the following equation:

$$p^P = \mathbf{T}_{W\leftarrow P}^{-1}\mathbf{T}_{W\leftarrow S}\mathbf{T}_{S\leftarrow I}\mathbf{T}_{scale}\,p^I \tag{1}$$

where $\mathbf{T}_{scale}$ is the scale matrix, which converts the unit of the point from pixel to metric units. It is determined by the ultrasound machine manufacturer and ultrasonic propagation medium. During the calibration process, sufficient point data were used in calculating the transformation matrix. Suppose the number of data points is n, the point p^P and p^I in Eq. (1) can be rewritten as X^P and X^I, which have the following matrix form:

$$X^P = \begin{pmatrix} x_1^P & \cdots & x_i^P & \cdots & x_n^P \\ y_1^P & \cdots & y_i^P & \cdots & y_n^P \\ z_1^P & \cdots & z_i^P & \cdots & z_n^P \\ 1 & \cdots & 1 & \cdots & 1 \end{pmatrix} \tag{2}$$

$$X^I = \begin{pmatrix} x_1^I & \cdots & x_i^I & \cdots & x_n^I \\ y_1^I & \cdots & y_i^I & \cdots & y_n^I \\ z_1^I & \cdots & z_i^I & \cdots & z_n^I \\ 1 & \cdots & 1 & \cdots & 1 \end{pmatrix} \tag{3}$$

Thus, Eq. (1) can be written as:

$$X^P = \mathbf{T}_{W\leftarrow P}^{-1}\mathbf{T}_{W\leftarrow S}\mathbf{T}_{S\leftarrow I}\mathbf{T}_{scale}X^I \tag{4}$$

Then, the calibration matrix can be solved using a straightforward implementation of the least mean squares algorithm. The transformations during ultrasound calibration are illustrated in Fig. 2.

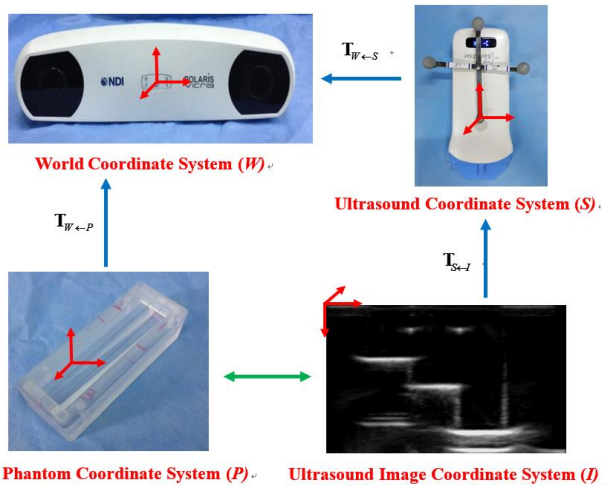

Fig. 2 Transformations during ultrasound calibration

2.3 Calibration principle of N-wedge phantom

The N-wedge phantom consists of three planes (Plane 1, 2, 3) and two lines (Line 1, 2), as shown in Fig. 3. The ultrasound image plane intersects three planes with three red lines, and two lines with two red points A_1, A_2. The coordinates of B_1 and C_1 in the phantom coordinate system are known in the phantom design process. Thus, the coordinates of P_1 in the phantom can be calculated as

$$P_1^P = (1-\alpha)B_1^P + \alpha C_1^P \tag{5}$$

where $\alpha = \frac{\|B_1^P - P_1^P\|}{\|B_1^P - C_1^P\|}$. According to the unique geometry structure, we know that line M_1B_1 is parallel to C_1N_1. Then, the ratio α can be calculated as $\alpha = \frac{\|M_1^P - P_1^P\|}{\|M_1^P - N_1^P\|}$. At the same time, the intersection lines and points of the ultrasound image plane with three wedges and two lines in the phantom will display three gray-intensity lines and two points in the ultrasound image, which can be segmented as three horizontal lines and two points. After image processing, the coordinates of point P_i, M_i, and N_i (i=1,2) can be acquired. It should be noted that the ratio α of the two distances is constant regardless of the coordinate system they are in. The ratio can also be calculated in the image coordinate system as follows, while the coordinates of P_1 can be calculated using Eq. (5).

$$\alpha = \frac{\|M_1^I - P_1^I\|}{\|M_1^I - N_1^I\|} \tag{6}$$

The coordinates of P_2 are also acquired by applying the same principle. Finally, the calibration matrix is solved in the closed-form algorithm after sufficient points data have been collected.

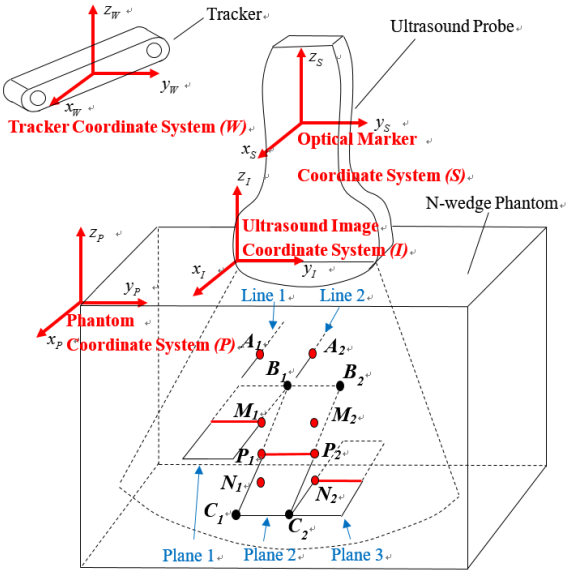

Fig. 3 Principle of N-wedge phantom. The N-wedge phantom consists of three planes and two lines. They are shown as three lines and two points in the corresponding ultrasound image. After ultrasound image segmentation, two target points are collected for calibration.

2.4 Ultrasound image segmentation

One of the advantages of ultrasound calibration based on the N-wedge phantom is that it reduces the difficulty of ultrasound image segmentation. In the traditional N-wire phantom, the wires are imaged as points in the image, while impurities in water are also imaged as speckles. As the number of wires in the N-wire phantom increases, the number of points in the image also increases steeply. Both the targets and noise are like circle-shaped dots, and they pose several challenges for the automatic image segmentation algorithm. However, the N-wedge phantom uses several wedges instead of wires, and it reduces the number of points in the ultrasound image. This design ensures that less difficulty is encountered in automatic image segmentation. Furthermore, as described in [13], automatic segmentation is feasible when N-wire phantoms are used because the intersection between the N-wire and the ultrasound image is shown in the image as three collinear bright spots. Although this geometric constraint makes the segmentation easier, it is logically more complicated than that of the N-wedge phantom.

The automatic image processing algorithm of the N-wedge phantom is illustrated as follows. The original ultrasound image is shown in Fig. 4(a). The image was divided into two parts for image processing, namely the point part and the line part. The point part is located in the upper part of the image, while the line part is in its lower part. The point part image was processed into a binary image with a threshold of 110. Then, it was eroded using a morphological circular structural element with a radius of 3 pixels. Next, the edges of the binary image were fitted with a circle and the coordinates of the point was determined as the circle center. The line part image was processed into a binary image with a threshold of 140. The morphological erosion of the line part image was carried out using a rectangular structural element with dimensions of 3×3

pixels. Next, for each column of pixels scanning from top to bottom, three line segments were detected and the remaining pixels after these positions were discarded. Then, each remaining line segment was fitted with a rectangle. A horizontal line was drawn through the center of each rectangle. The results of the point part and the line part image are shown in Fig. 4(b). Next, two lines were drawn from the above two points, perpendicular to the three horizontal lines (Fig. 4(c)) and the coordinates of six points were determined (Fig. 4(d)). Thus, α can be calculated using Eq. (6). After image processing, two points can be used for calibration in each ultrasound image.

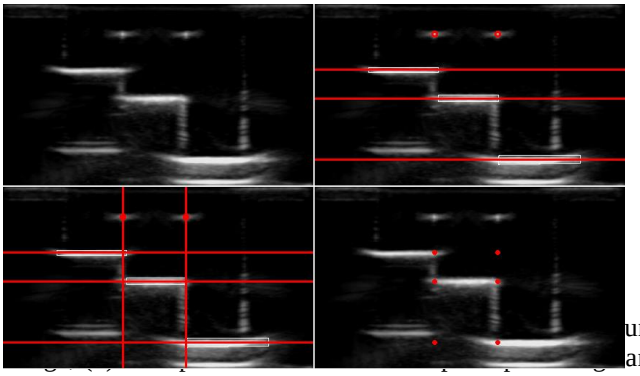

und
and three lines are found for the line part image; (c) Two vertical lines are found according to the two points and three lines; (d) Six intersection points are found and two target points can be used for calibration.

3 Results

Several values were obtained after a set of calibration experiments for the N-wedge phantom and N-wire phantom. The two phantoms were both filled with water. According to [24], the ultrasound segmentation algorithm shifts the segmented points and lines toward the ultrasound probe by the factor Swater/1540 (Swater is the speed of sound in water) to remove error due to the difference in the speed of sound in water and soft tissue.

To evaluate the performance of the N-wedge phantom, the calibration results were compared with those of the N-wire phantom in terms of precision, accuracy, calibration time, ease of use, and manufacture.

3.1 Precision

To determine the precision of the calibration methods, N results are required from the independent calibration experiments, that is, $\mathbf{T}_{S\leftarrow I_i}, i=1,...,N$. The center point and four corner points are mapped from the image frame to the probe frame using the N calibration results. This method of calculating the precision is called calibration reproducibility (CR). The method does not include image alignment and segmentation errors. It is often computed as follows [2]:

$$\mathrm{CR}=\frac{1}{N}\sum_{i=1}^{N}\left\|\mathbf{T}_{S\leftarrow I_i}\mathbf{T}_{scale}p^{I}-\bar{p}^{S}\right\| \tag{7}$$

where

$$\bar{p}^{S}=\frac{1}{N}\sum_{i=1}^{N}\left\|\mathbf{T}_{S\leftarrow I_i}\mathbf{T}_{scale}p^{I}\right\| \tag{8}$$

The precision was evaluated for both the N-wire phantom and the N-wedge phantom. The calibration reproducibility was calculated at the center and the average (center and four corners) of the image using 10 independent calibration results. The results are summarized in Table 1.

Table 1 Precision analysis at the center and the average of the image

	Center	Average
N-wire (mm)	0.74±0.34	0.89±0.45
N-wedge (mm)	0.67±0.36	0.81±0.39

3.2 Accuracy

To evaluate the accuracy of the calibration methods, N results from the independent calibration experiments are also required. A point target in the phantom coordinate system can be determined by the intersection point of a pair of cross-wire. The location of the point can be acquired using a stylus. A stylus is a commonly used tool in medical application, which has several optical markers on it. Before the calibration experiments, the stylus was calibrated with a root-mean calibration error of 0.64 mm. The location of the target point can be determined using a series of coordinate transformations. After determining the points in the phantom coordinate system, an ultrasound image of the point target was captured, and its image coordinates were acquired by manual image segmentation. The accuracy was determined by calculating the point reconstruction accuracy (PRA) as follows [2]:

$$PRA=\left\|p^{P}-\mathbf{T}_{P\leftarrow W}\mathbf{T}_{W\leftarrow S}\mathbf{T}_{S\leftarrow I}\mathbf{T}_{scale}p^{I}\right\| \tag{9}$$

The PRA test results obtained at the center and the average (center and four corners) of the image are summarized in Table 2, which contains results for the N-wire phantom and N-wedge phantom.

Table 2 Accuracy analysis at the center and the average of the image using cross-wire phantom

	Center	Average
N-wire (mm)	1.89±0.42	2.10±0.51
N-wedge (mm)	1.73±0.48	1.95±0.56

3.3 Image segmentation time

The average time required to segment a single image in automatic ultrasound image segmentation of the N-wire phantom has been reported to be 0.17 s [13]. In contrast, the average ultrasound image processing time of the N-wedge phantom is approximately 0.012 s per image. Furthermore, the recognition accuracy rate of ultrasound image processing of the N-wedge can be up to 92% in each group of 15 experiments. The segmentation time of other calibration methods can be determined using fCal software, which is freely available in the PLUS (Public software Library for UltraSound image

research) toolkit developed by the Perklab group at Queen's University [25].

3.4 Ease of use

As previously described, the user needs to use a stylus to select some points on the N-wire phantom before calibration. This is a time-consuming process and difficult for the user to operate. However, several positioning holes in the N-wedge phantom can assist the user in locating the selected points, as shown in Fig. 5. The purpose of the positioning holes of the N-wedge phantom is to calculate the coordinate transformation from the model coordinate system to the reference coordinate system. The model coordinate system is used when designing the phantom using NX 3D design software. The reference coordinate system is the coordinate system of the phantom after the phantom and the optical markers are fixed together. At least three points are required to complete the coordinate transformation of these two coordinate systems. The positioning holes are used to collect the data points.

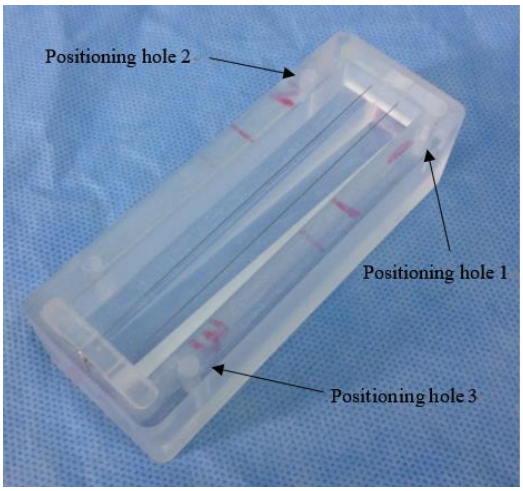

Fig. 5 N-wedge phantom. It has three positioning holes, which are used to calculate the coordinate system transformation from the model coordinate system to the reference coordinate system, and the holes ensure ease of operation.

3.5 Phantom manufacture

Our N-wire phantom and N-wedge phantom were both made of plexiglass using engraving machine (Roland, Japan). The N-wire phantom was divided into multiple parts in the process and should be assembled together in the end. The most difficult part of its manufacturing process was drilling of 12 small through holes in the phantom and passing 6 nylon lines through these holes. In contrast, 4 small holes were drilled in the N-wedge phantom and 2 nylon lines were passed through the holes. The three planes of the N-wedge phantom were designed as one whole part using NX 3D design software without additional manufacturing complexity.

4 Discussion

It can be observed from Table 1 and Table 2 that the precision and accuracy of the N-wedge phantom and N-wire phantom are comparable. The reason is that the N-wedge phantom is made of planes and wires, which appears as lines and points in the ultrasound image. The line is segmented easily and accurately in the ultrasound image. It can also be observed from Table 1 that the precision at the center of the image is better than that of the average points of the image in both the N-wire and N-wedge phantoms. A possible reason is that there is an error in the rotation part of the calibration matrix so that the corners of the image are incorrect after transformation from the image frame to the probe frame. The factors that may lead to calibration error in the N-wire phantom include segmentation error, phantom manufacturing error, phantom production accuracy, tracking accuracy, and user intervention.

Although the most important calibration factors are precision and accuracy, there are other aspects that should be noted during the calibration. First, a stylus is used to accurately locate the position of some important points in the N-wire phantom, which is a boring and cumbersome process for users. In contrast, it is easy and convenient to use a stylus in the N-wedge phantom because there are positioning holes to assist the stylus in selecting the points. Second, during the calibration process, the ultrasound probe scans the phantom manually so that a clear ultrasound image can be acquired. The N-wedge phantom is made of fewer wires than the N-wire phantom; therefore, clear ultrasound images are obtained conveniently, which can be easily segmented for calibration. Furthermore, the image segmentation time of the N-wedge phantom is shorter. Third, the N-wedge phantom and N-wire phantom are both produced using engraving machine. According to our production experience, more time was spent on the N-wire phantom than the N-wedge phantom. Table 3 lists the factors considered for our phantoms, while Table 4 lists the same factors for other existing phantoms.

Table 3 Ultrasound calibration factors for N-wire phantom and N-wedge phantom

Factor	N-wire phantom	N-wedge phantom
Precision (mm)	0.74±0.34	0.67±0.36
Accuracy (mm)	1.89±0.42	1.73±0.48
Image segmentation time (s)	-	0.012
Ease of use	Easy	Very easy
Phantom manufacture	Moderate	Easy

Table 4 Ultrasound calibration factors for other existing phantoms

Factor	N-wire phantom [13]	N-wire phantom [22]	Cambridge [10]
Precision (mm)	0.66	0.5	0.88

Accuracy (mm)	-	1.4	1.67
Image segmentation time (s)	0.17	-	-
Ease of use	-	-	Difficult
Phantom manufacture	-	-	Moderate

5 Conclusion

The N-wedge phantom was proposed in this paper and compared with the traditional N-wire phantom in terms of factors such as precision, accuracy, calibration time, ease of use, and manufacture. The precision and accuracy of the two phantoms met the requirements for medical application. The N-wedge phantom has the advantage that a line is easier and more accurately segmented from the ultrasound image than a point so that the axial direction of the ultrasound image can be accurately located, which improves calibration accuracy. Calibration error may be due to probe alignment error, phantom production accuracy, tracking accuracy, and user intervention. The calibration process using the N-wedge phantom is also easy and simple for new users, and it can be easily manufactured.

6 Acknowledgements

This study was funded by the National Natural Science Foundation of China (Grant Nos. 51205250 and 51575343).

7 References

[1] Fenster, A., Downey, DB., Cardinal, HN.: 'Three-dimensional ultrasound imaging', Phys. Med. Biol., 2001, 46, (5), pp. 67-99

[2] Hsu, P.: 'Freehand three-dimensional ultrasound calibration'. PhD thesis, University of Cambridge, 2008

[3] Gee, A., Prager, R., Treece, G., Berman, L.: 'Engineering a freehand 3D ultrasound system', Pattern Recognit. Lett., 2003, 24, (4-5), pp. 757-777

[4] Mercier, L., Langø, T., Lindseth, F., Collins, LD.: 'A review of calibration techniques for freehand 3-D ultrasound systems', Ultrasound Med. Biol., 2005, 31, (2), pp. 143-165

[5] Melvær, EL., Mørken, K., Samset, E.: 'A motion constrained cross-wire phantom for tracked 2D ultrasound calibration', Int. J .Comput. Assist. Radiol. Surg., 2012, 7, (4), pp. 611-620

[6] Brendel, B., Winter, S., Ermert, H.: 'A simple and accurate calibration method for 3D freehand ultrasound', Biomed. Tech., 2004, 42, (2), pp. 872-873

[7] Bø, LE., Hofstad, EF., Lindseth, F., et al: 'Versatile robotic probe calibration for position tracking in ultrasound imaging', Phys. Med. Biol., 2005, 60, (9), pp. 3499-3513

[8] Leotta, DF.: ' An efficient calibration method for freehand 3-D ultrasound imaging systems', Ultrasound Med. Biol., 2004, 30, (7), pp.999-1008

[9] Carr, J.: 'Surface reconstruction in 3D medical imaging'. PhD thesis, University of Canterbury,1996

[10] Prager, RW., Rohling, RN., Gee, AH., et al: 'Rapid calibration for 3-D freehand ultrasound', Ultrasound Med. Biol., 1998, 24, (6), pp.855-869

[11] Comeau, RM., Fenster, A., Peters, TM.: 'Integrated MR and ultrasound imaging for improved image guidance in neurosurgery' (Proceedings The International Society for Optical Engineering: Medical Imaging, 1998), pp. 747-755

[12] Hsu, PW., Prager, RW., Gee, AH., et al: 'Real-time freehand 3D ultrasound calibration', Ultrasound Med. Biol., 2008, 34, (2), pp.239-251

[13] Chen, TK., Thurston, AD.，Ellis, RE.，et al: 'A real-time freehand ultrasound calibration system with automatic accuracy feedback and control', Ultrasound Med. Biol., 2009, 35, (1), pp.79-93

[14] Peterhans, M., Anderegg, S., Gaillard, P., et al: 'A fully automatic calibration framework for navigated ultrasound imaging' (IEEE Engineering in Medicine and Biology Society, 2010), pp. 1242-1245

[15] Rousseau, F., Hellier, P., Barillot, C.: 'Confhusius: a robust and fully automatic calibration method for 3D freehand ultrasound', Med. Image. Anal., 2005, 9, (1), pp.25-38

[16] Hsu, PW., Prager, RW., Gee, AH., et al: 'Rapid, easy and reliable calibration for freehand 3D ultrasound', Ultrasound Med. Biol., 2006, 32, (6), pp.823-835

[17] Najafi, M., Afsham, N., Abolmaesumi, P., et al: 'A closed-form differential formulation for ultrasound spatial calibration: multi-wedge phantom', Ultrasound Med. Biol., 2014, 40, (9), pp.2231-2243

[18] Najafi, M., Afsham, N., Abolmaesumi, P., et al: 'A closed-form differential formulation for ultrasound spatial calibration: single wall phantom', Ultrasound Med. Biol., 2015, 41, (4), pp.1079-1094

[19] Thomas, L.: 'Ultrasound guided surgery: image processing and navigation'. PhD thesis, Norwegian University of Science and Technology, 2000

[20] Muratore, DM., Galloway, RL.:'Beam calibration without a phantom for creating a 3-D freehand ultrasound system', Ultrasound Med. Biol., 2001, 27, (11), pp.1557-1566

[21] Hsu, PW., Treece, GM., Prager, RW., et al: 'Comparison of freehand 3-D ultrasound calibration techniques using a stylus', Ultrasound Med. Biol., 2008, 34, (10), pp.1610-1621

[22] Carbajal, G., Lasso, A., Gómez, A.,et al: ' Improving N-wire phantom-based freehand ultrasound calibration', Int. J. Comput. Assist Rad. Surg., 2013, 8, (6), pp.1063-1072

[23] Comeau, RM., Sadikot, AF., Fenster, A., et al: 'Intraoperative ultrasound for guidance and tissue shift correction in image-guided neurosurgery', Med. Phys., 2000, 27, (4), pp.787-800

[24] Hsu, PW., Prager, RW., Gee, AH., et al: ' Real-time freehand 3D ultrasound calibration', Ultrasound Med. Biol., 2008, 34, (2), pp.239-251

[25] Lasso, A., Heffter, T., Rankin, A., et al: 'Plus: open-source toolkit for ultrasound-guided intervention systems', IEEE Trans. Biomed. Eng., 2014, 61, (10), pp.2527-2537